Cell Calcium 56 (2014) 157–168

Contents lists available at ScienceDirect

Cell Calcium

journal homepage: www.elsevier.com/locate/ceca

Termination of calcium puffs and coupled closings of inositol trisphosphate receptor channels

Steven M. Wiltgen[a,1], George D. Dickinson[a,*,1], Divya Swaminathan[a], Ian Parker[a,b]

[a] Department of Neurobiology & Behavior, University of California, Irvine, CA 92697, USA
[b] Department of Physiology & Biophysics, University of California, Irvine, CA 92697, USA

ARTICLE INFO

Article history:
Received 3 April 2014
Received in revised form 6 June 2014
Accepted 16 June 2014
Available online 26 June 2014

Keywords:
Calcium
Coupled gating
Inositol 1,4,5-trisphosphate receptors
Puffs
TIRF microscopy

ABSTRACT

Calcium puffs are localized Ca^{2+} signals mediated by Ca^{2+} release from the endoplasmic reticulum (ER) through clusters of inositol trisphosphate receptor (IP_3R) channels. The recruitment of IP_3R channels during puffs depends on Ca^{2+}-induced Ca^{2+} release, a regenerative process that must be terminated to maintain control of cell signaling and prevent Ca^{2+} cytotoxicity. Here, we studied puff termination using total internal reflection microscopy to resolve the gating of individual IP_3R channels during puffs in intact SH-SY5Y neuroblastoma cells. We find that the kinetics of IP_3R channel closing differ from that expected for independent, stochastic gating, in that multiple channels tend to remain open together longer than predicted from their individual open lifetimes and then close in near-synchrony. This behavior cannot readily be explained by previously proposed termination mechanisms, including Ca^{2+}-inhibition of IP_3Rs and local depletion of Ca^{2+} in the ER lumen. Instead, we postulate that the gating of closely adjacent IP_3Rs is coupled, possibly via allosteric interactions, suggesting an important mechanism to ensure robust puff termination in addition to Ca^{2+}-inactivation.

Published by Elsevier Ltd.

1. Introduction

Puffs and sparks are archetypical examples of transient, localized subcellular Ca^{2+} signals. They are generated by Ca^{2+} liberation from the endo/sarco-plasmic reticulum (ER/SR) through the coordinated openings of small numbers of clustered inositol trisphosphate receptor (IP_3R) or ryanodine receptor (RyR) channels, respectively [1,2]. IP_3Rs and RyRs share considerable sequence homology [3], and share a crucial functional characteristic in that their opening is promoted by moderate elevations of cytosolic $[Ca^{2+}]$ [4–6], thereby creating a positive feedback loop of Ca^{2+}-induced Ca^{2+} release (CICR) such that opening of one channel promotes the opening of neighboring channels. The concerted opening of multiple channels during puffs and sparks may thus be readily explained by the rapid diffusion of Ca^{2+} ions within a cluster to activate neighboring channels by CICR [7]. However, because CICR is an intrinsically self-reinforcing process it is less clear what mechanisms then "put out the fire" [8] to terminate puffs and sparks, which typically have durations of only a few tens of milliseconds [2,9].

This has been a particularly vexing question in the case of sparks because, unlike the IP_3R, in vitro studies of RyRs have failed to reveal any strong Ca^{2+}-dependent inhibition mechanism [10–14]. The issue remains unresolved [15], but several possibilities have been proposed [8] which, in principle, may be involved in the termination of both puffs and sparks. (1) *Stochastic attrition*. Given the stochastic nature of channel gating, there is always a chance that all channels within a cluster will happen to be closed at the same time, breaking the feedback loop and extinguishing Ca^{2+} liberation. However, the probability of this happening becomes vanishingly small with increasing numbers of channels, rendering stochastic attrition unviable as the sole termination mechanism for clusters containing more than a few active channels. (2) *Local depletion*. This mechanism invokes a local reduction of Ca^{2+} stores within the ER or SR lumen during puffs or sparks, so that release events terminate either directly because the Ca^{2+} flux through open channels drops sufficiently to break the positive feedback loop of CICR [15], or indirectly through modulation of channel gating via putative Ca^{2+} binding sites on the luminal face of the receptor [12]. (3) *Coupled gating of channels*. Lipid bilayer recordings have shown that multiple RyRs may synchronize their openings so as to appear as a single channel of multi-fold conductance [16,17]. Such allosteric coupled gating is an appealing mechanism to

* Corresponding author. Tel.: +1 9498247833
E-mail addresses: dickinsg@uci.edu, george.dickinson@gmail.com (G.D. Dickinson).
[1] These authors contributed equally to this work.

http://dx.doi.org/10.1016/j.ceca.2014.06.005
0143-4160/Published by Elsevier Ltd.

synchronize the closing of multiple, neighboring channels within a cluster, but its role in spark termination remains speculative [8].

Different from RyRs, the gating of IP_3R channels is biphasically dependent on cytosolic $[Ca^{2+}]$. Elevations of up to one or a few μM promote channel opening, whereas higher concentrations rapidly cause inhibition [3,18]. Given that Ca^{2+} concentration in the close vicinity of open IP_3R channels likely rise to several tens of μM or greater [19], Ca^{2+}-dependent inhibition is believed to play a major role in puff termination [7]. Indeed, several theoretical studies have shown that simulations of clustered IP_3Rs incorporating positive and negative feedback of cytosolic Ca^{2+} on channel gating exhibit stochastic excitability where channels open and close in a concerted fashion reminiscent of puffs [7,20–23]. However, a wide range of variability in affinity and rate of inactivation has been reported across different IP_3R subtypes [3,24–26], and the ability of model simulations to replicate puffs depends on these and other poorly-characterized parameters, such as the channel spacing within clusters and the influence of endogenous cytosolic buffers on Ca^{2+} diffusion and chelation. It thus remains unclear whether Ca^{2+} inactivation provides sufficient negative feedback to enable puff termination in vivo.

Until recently, technical limitations have hampered experimental investigation of puff termination mechanisms because available imaging techniques (primarily linescan confocal microscopy) could not resolve the contributions of individual IP_3R channels. By using total internal reflection fluorescence (TIRF) microscopy to monitor signals from attoliter volumes around puff sites in conjunction with cytosolic loading of the slow Ca^{2+} buffer EGTA we are now able to obtain fluorescence records from intact cells that closely approximate the instantaneous Ca^{2+} flux (Ca^{2+} current) through single and clustered IP_3R channels [9]. This technique of 'optical patch-clamping' [27] yields traces closely resembling electrophysiological patch-clamp recordings, and reveals step-wise transitions during puffs that reflect the openings and closings of individual channels [9]. In this respect, the longer durations of puffs (~100 ms) makes them more amenable to experimental studies than the much briefer (~10 ms) sparks, where the durations of channel openings cannot be directly resolved but is generally inferred from the rise time of the fluorescence signal [15].

Here, we present findings that the termination of Ca^{2+} puffs involves temporally correlated closings of adjacent IP_3R channels within a cluster. Different from this, model simulations wherein IP_3Rs can interact only via cytosolic Ca^{2+} predict that channel closings should be substantially independent of one another. We thus propose that puff termination involves a further mechanism beyond Ca^{2+}-mediated inhibition, possibly mediated by allosteric interaction between closely adjacent IP_3R channels and analogous to that described for RyRs.

2. Materials and methods

2.1. Cell preparation and imaging

Experiments were performed on human neuroblastoma SH-SY5Y cells, using procedures as previously described [9] except that fluo-8 was used as the calcium indicator. We find that fluo-8 provides a brighter fluorescence signal and better signal-to-noise ratio than fluo-4, which we had used previously, but that fluorescence ratio signals ($\Delta F/F_0$) associated with blips and puffs are closely similar between the two indicators. In brief, cells were loaded with caged iIP_3, fluo-8, and EGTA by bath incubation with membrane-permeant esters. Imaging of local $[Ca^{2+}]_i$ signals was accomplished using a home-built TIRF microscope system based around an Olympus IX 70 microscope equipped with an Olympus 60x NA 1.45 TIRFM objective [9]. Fluorescence of cytosolic fluo-8 was excited within the ~100 nm evanescent field formed by total internal reflection of a 488 nm laser beam at the coverglass/aqueous interface. Images of emitted fluorescence ($\lambda > 510$ nm) were captured at a resolution of 128×128 pixels (1 pixel = 0.33 μm) at 420 frames s^{-1} by a Cascade 128 electron-multiplied CCD camera (Roper Scientific). Native IP_3Rs in SH-SY5Y cells were activated by photorelease of iIP_3 from a caged precursor by flashes of UV (350–400 nm) light focused uniformly across the imaging field. Fluorescence pseudoratio image stacks ($\Delta F/F_0$) were created using the MetaMorph software package (Molecular Dynamics), and fluorescence traces of local Ca^{2+} signals were obtained by measuring fluorescence ratio changes within 3×3 pixel (1×1 μm) regions of interest centered on puff and blip sites. The membrane permeant caged IP_3 analog ci-IP_3/PM was purchased from SiChem (Bremen, Germany). EGTA-AM was from Invitrogen (Carlsbad, CA), and fluo-8 AM from ABD Bioquest (Sunnyvale, CA). All other reagents were purchased from Sigma (St. Louis).

2.2. Puff simulations

For comparison with experimental data, we modeled IP_3R kinetics during puffs using two schemes; (i) assuming that channel closings were completely independent, and (ii) allowing the possibility that channel closings are modulated by Ca^{2+}-mediated interactions among receptors within a cluster.

In the independent closings model (IC) we considered IP_3R kinetics as a simple two-state Markovian model [28]. Transition from the open to the closed state is determined only by the rate constant $k_{off} = 1/\tau_{open}$, which is the same for all channels; i.e. the mean open dwell time of a channel is independent of the state of other channels in the cluster.

We also modeled IP_3R kinetics using the De Young–Keizer scheme (DYK) in conjunction with a point source approximation for determining the concentration of calcium seen by channels within a cluster following channel opening [29,30]. All channels in the cluster are thus exposed to the same calcium concentration; an arrangement that would maximize Ca^{2+}-mediated interactions among receptors as compared to a model in which IP_3Rs were more widely distributed throughout a cluster. Simulations were performed for given numbers, n, of channels within a cluster. At time $t = 0$ all channels were set to their open state, and the system was then allowed to evolve stochastically. To derive the model data in Fig. 5B we corrected simulated traces of channel openings by disregarding closings <10 ms so as to eliminate brief 'flickers' that would not be resolved in the optical recordings, and excluded from analysis all recordings in which a channel re-opened after having remained closed for >10 ms, to accord with our selection of experimental data where puffs were excluded if they showed evident re-openings during their falling phase. For the analysis in Fig. 7D–G idealized recordings of the number of open channels as a function of time were processed to accord more closely with the experimental recordings by smoothing via adjacent-averaging (10-point weighted average; 0.5 ms per point) followed by addition of Gaussian noise with a standard deviation matching the experimental recordings (Figs. 1D and E and 7G–I).

3. Results

3.1. Inferring single-channel IP_3R dynamics from fluorescence recordings

We imaged Ca^{2+} fluorescence signals using TIRF microscopy in SH-SY5Y neuroblastoma cells loaded with fluo-8, caged iIP_3 and EGTA; the latter used to localize Ca^{2+} signals and inhibit propagation of Ca^{2+} waves [9]. Photorelease of iIP_3 by a UV light flash

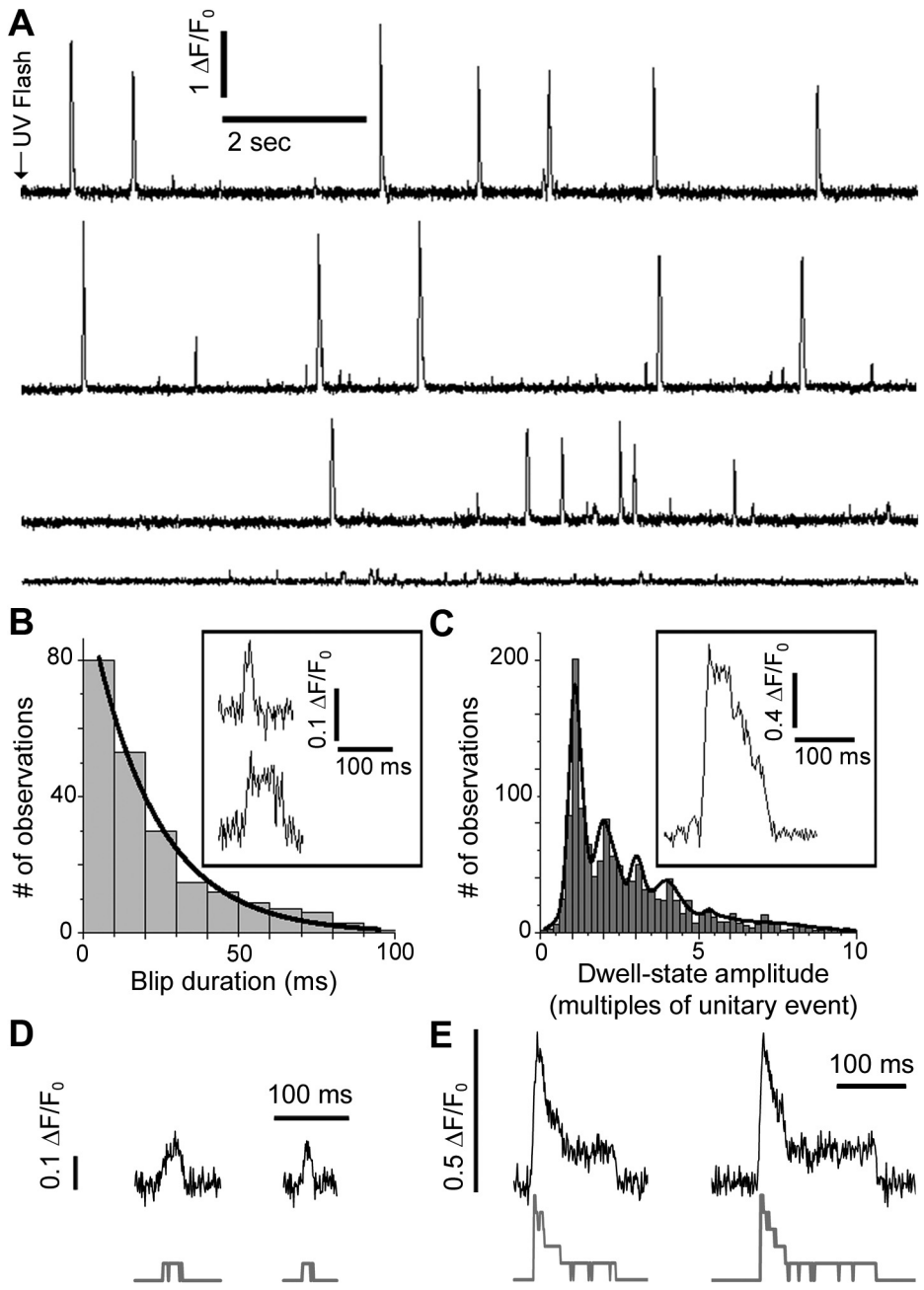

Fig. 1. Resolution of single IP_3R channel Ca^{2+} signals during puffs and blips. (A) Representative traces of Ca^{2+}-fluorescence from sites in 4 different cells showing activity following photorelease of iIP_3. The upper 3 traces show both puffs and blips, whereas the lower trace is from a site that generated only blips. (B) The graph plots the distribution of blip durations ($n = 216$ events, 36 sites). The curve is a single exponential fitted to the data with time constant = 21 ms. The inset illustrates two examples of blips on an expanded time scale. (C) Unitary, stepwise decrements during the falling phase of puffs. The inset trace shows a single puff on expanded timescale, illustrating abrupt transitions between dwell-state levels on the falling phase. The graph plots the distribution of visually identified dwell-state amplitudes from 228 puffs, scaled as multiples of the mean unitary single-channel (blip) amplitude ($\Delta F/F_0 = 0.11$). The curve is a multi-Gaussian distribution fitted to the data. (D–E) Computer-generated traces illustrating how the fluorescence traces may relate to underlying IP_3R channel gating. Lower, gray traces depict simulated channel openings generated by a De Young–Keizer IP_3R model containing a single channel (D) and a 'point source' cluster of 5 channels (E). Upper, black traces show corresponding traces, simulated by smoothing and adding Gaussian noise to approximate experimental fluorescence recordings. The units of fluorescence were based on a mean blip amplitude ($\Delta F/F_0 = 0.11$).

evoked repetitive Ca^{2+} signals at several discrete sites within a cell, and activity persisted for a few minutes after the flash (e.g. Fig. 1A). Events were of highly variable peak amplitudes, varying from unitary 'blips' (lower trace, Fig. 1A; inset, Fig. 1B) thought to arise from openings of single IP_3R channels to large puffs (upper traces, Fig. 1A; inset Fig. 1C) that may involve the simultaneous opening of several channels [9]. Much of this variability arises from differences in the numbers of functional IP_3R present at different cluster sites [30].

Puffs and blips imaged by TIRF microscopy in EGTA-loaded cells display abrupt transitions between fluorescence levels, indicating that the fluorescence signals track channel openings and closings with a temporal blurring of only a few ms [19,39]. In particular, puffs display step-wise, abrupt transitions between fluorescence levels, predominantly during their falling phase (e.g. inset, Fig. 1C), and the distribution of these levels is multi-modal with recurring peaks at integer multiples of the unitary blip amplitude [9] (Fig. 1C). We had previously concluded that these transitions in amplitude levels reflect step-wise recruitment and closing of varying numbers of IP_3Rs [9] localized within clusters with dimensions of <400 nm [31]. Similarly, measurements of blip durations provide

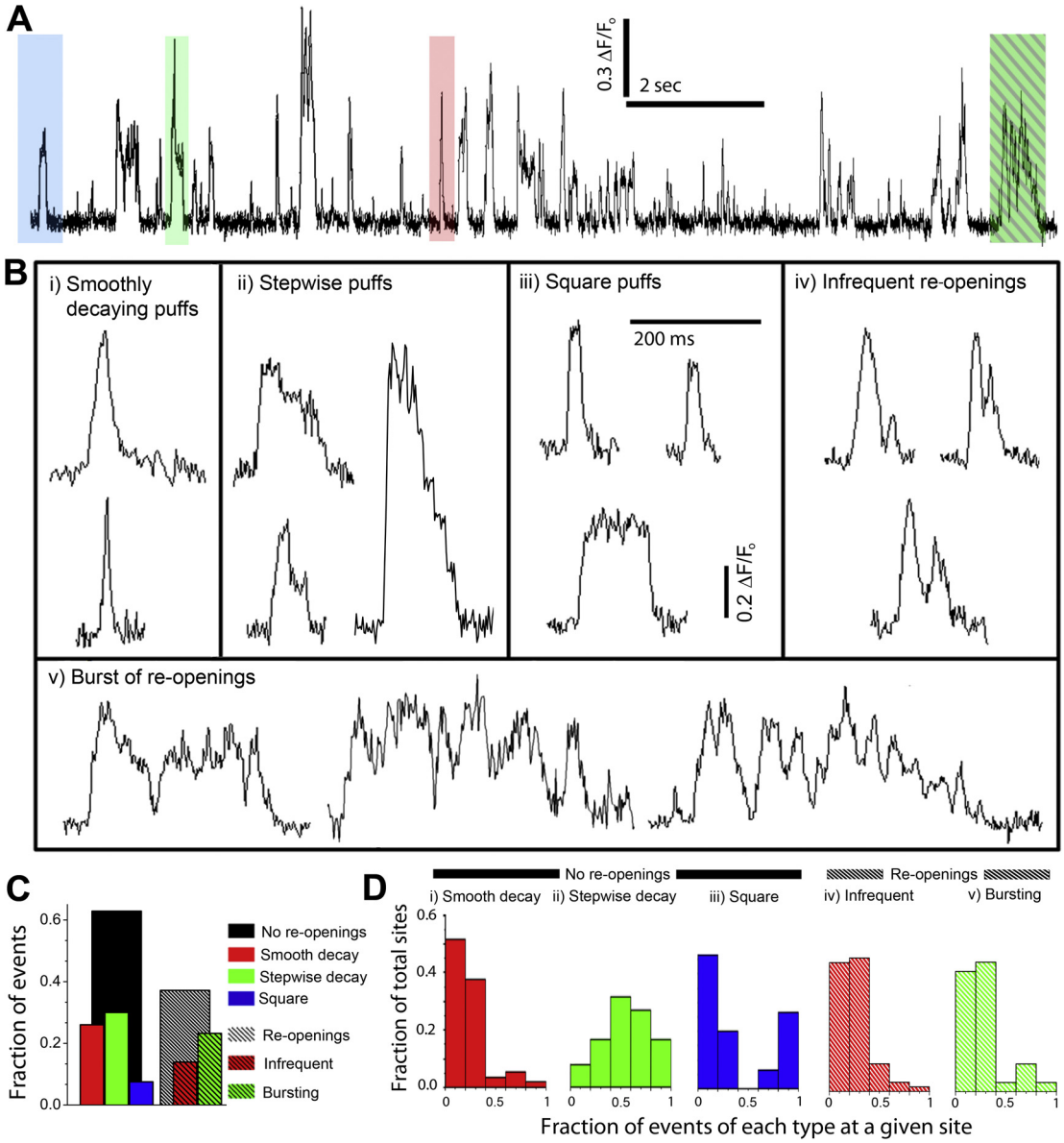

Fig. 2. Differing temporal morphologies of puffs. (A) Recording from a single puff site that displayed a wide variety of puff morphologies. Colored boxes highlight puffs showing 'square' (blue), stepwise (green) and smoothly decaying (red) time courses, together with an event displaying burst-like re-openings (green hatched). (B) A bestiary of puff morphologies. Each box shows three examples of puffs subjectively classified as: (i) smoothly decaying; (ii) showing stepwise decays; (iii) with 'square' morphology; (iv) having infrequent re-openings; and (v) showing multiple bursts of re-openings. Scale bars are applicable to all panels. (C) Overall proportions of puffs showing different morphologies. Black bars show the fraction of events without (solid bar: 63%) and with re-openings (hatched bar: 37%). Colored bars show the corresponding fractions of events with and without re-openings that were classified as smoothly decaying (red), with stepwise decay (green) and square (blue). (D) The histogram in each panel plots the fraction of the total puff sites that displayed a given proportion of puffs of each morphology (labeled i–v, as in *B*). Data in C and D are derived from measurements of 774 puffs at 94 sites.

an estimate of the open times of single IP_3R channels, which follow an approximately exponential distribution (Fig. 1B). However, fine details of gating kinetics may be lost, owing to the temporal filtering and noise level of the fluorescence recordings. We illustrate this in Fig. 1D and E, showing idealized records of channel openings generated by a De Young–Keizer IP_3R model [29,30], together with corresponding fluorescence traces simulated by assuming the optical recording approximates a weighted 10-point (0.5 ms per point) smoothing of the channel traces with added noise. Although brief 'flickers' to closed states in the channel traces were poorly resolved in the simulated fluorescence traces, the optical recordings nevertheless provided a good estimate of the burst durations for which individual channels remained open.

3.2. Diverse temporal morphologies of puffs

We observed marked qualitative differences among time courses of puffs, both between different events at a given site (e.g. Fig. 2A), and between sites. To quantify the proportions of puffs with differing temporal morphologies we subjectively classified events into five categories, based on the shape of their falling phases (Fig. 2B): (i) smoothly decaying puffs, without discernible steps; (ii) puffs showing distinct stepwise decrements; (iii) 'square' puffs that terminated abruptly following a maintained plateau; (iv) puffs where the falling phase was interrupted by brief re-openings; (v) bursts of activity with multiple re-openings.

In all cases we expect that puffs would show abrupt transitions corresponding to closings of individual channels. Our

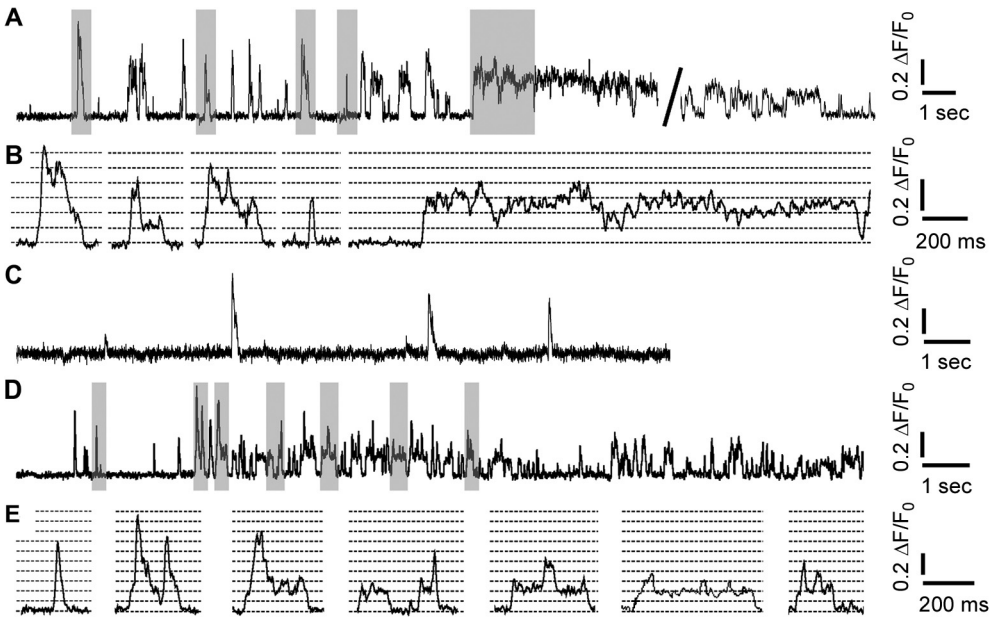

Fig. 3. Spontaneous failures of puff termination. (A) Fluorescence trace from a puff site that showed an abrupt change in behavior about 10 s after photorelease of IP_3, when transient puffs were replaced by a sustained Ca^{2+} liberation. This activity persisted for about 15 s (break in the trace marks an interval of ~5 s), before reverting to more normal puff activity. (B) Selected events marked by gray boxes in A, shown on an expanded time scale. Horizontal dashed lines correspond to integer multiples of the fluorescence level corresponding to single channel openings. (C) Simultaneous recording from a different site in the same cell, which continued to generate normal, transient puffs throughout the duration of the recording. (D) Fluorescence trace from a puff site in a different cell which displayed a transition from normal puff activity to sustained activity at a two-channel level. (E) Selected events from D, indicated by gray boxes, shown on an expanded time scale. Horizontal dashed lines correspond to integer multiples of the fluorescence level corresponding to single channel openings.

failure to discern steps in the smoothly-decaying puffs thus likely arose because of limited temporal resolution and noise of the fluorescence recordings. Concordant with this explanation, smoothly-decaying puffs showed atypically fast decays ($\tau = 7.8 \pm 0.52$ ms, $n = 20$ smoothly decaying puffs) on which it would be difficult to discern inflexions.

Fig. 2C shows the fractions of events from a total data set of 774 puffs that were classified as showing the different morphologies. We first grouped according to events with (63% of total: solid black bar) and without (37%: hatched black bar) re-openings. We then broke out the fractions of smoothly decaying (red bars), stepwise decaying (green) and square events (blue) within the no re-openings group, and the fractions of events showing infrequent or bursting re-openings. Among the puffs without re-openings, roughly equal proportions did or did not display clearly resolved steps on the falling phase (respectively, 29% and 26% of all events; red and green bars), and about 6% of all puffs showed 'square' morphology (blue bar). Among the puffs with re-openings, a greater proportion showed bust-like activity (green hatched bar) as compared to infrequent re-openings (red hatched bar).

Although a given puff site could display events of all five morphologies (e.g. Fig. 2A), it was apparent that particular sites often exhibited a preponderance of puffs of a given type. We examined this further in Fig. 2D, plotting in each panel the fraction of the total sites that displayed different proportions of puffs of a given morphology. Considering first the smoothly decaying puffs without visible steps, most sites showed only a small proportion of these events (Fig. 2D,i). In contrast, most sites showed a high proportion of stepwise puffs (Fig. 2D,ii). The distribution of 'square' puffs was markedly bimodal: most sites showed few or no square events, but at other sites a majority of events were square puffs (Fig. 2D,iii). Puffs with infrequent re-openings (Fig. 2D,iv) and bursts of re-openings (Fig. 2D,v) both, on average, made up only a small proportion of events at a given site.

3.3. Spontaneous failure of puff termination

At almost all of the thousands of sites from which we have recorded, puffs terminated within a few hundred ms and the fluorescence returned to baseline before the next event. However, on rare occasions we observed cases where the termination mechanism appeared to spontaneously fail, such that a localized puff site showed sustained Ca^{2+} liberation lasting for many seconds. Although we do not understand the reason for this, such instances provide important clues as to the nature of the termination mechanism.

One example is shown in Fig. 3A. Following photorelease of IP_3 the fluorescence trace showed a sequence of 'normal' puffs which continued for ~12 s. However, the behavior of the puff site then spontaneously and abruptly changed, so that instead of terminating after discrete events, Ca^{2+} release was sustained for nearly 15 s before reverting to a more typical pattern. The initial part of this transition is plotted on an expanded timescale in Fig. 3B, showing that the fluorescence signal appeared to 'latch up' to a level suggesting that fluctuating numbers of 1–4 IP_3R channels remained constitutively active. This behavior was unique to this particular puff site in the cell, because the basal Ca^{2+} level elsewhere in the cytosol remained unchanged and other puff sites showed no change in activity (Fig. 3C). Fig. 3D and E illustrates a further example of a somewhat different behavior at another a puff site, where normal puff activity transitioned for several seconds to a state where it appeared that two channels latched open intermittently for several hundred ms, with superimposed transient openings of additional channels.

We interpret these prolonged events as arising from a change in gating characteristics of IP_3Rs at a puff site, rather than from openings of some other type of channel. Specifically, they were observed only at sites that previously gave 'normal' puffs: consistent with a change in activity of those IP_3R channels that generated the puffs, but not, for example, with activation of store-operated channels responding to a generalized depletion of ER Ca^{2+}. Moreover, the

sustained activity showed fluorescence step levels matching those of the preceding puffs: again consistent with a change in open probability of the same channels that initially generated the normal puffs, but inconsistent with openings of plasmalemmal CRAC (ORAI) channels which individually have exceedingly low Ca conductance and would thus not be expected to generate discrete step levels in the fluorescence recording.

We thus conclude that, although robust, puff termination must involve some discrete mechanism that is subject to occasional failure; and that in such situations one or more IP_3R channels continue to liberate Ca^{2+} for prolonged periods. The observation that the fluorescence amplitudes showed only a slight decline over several seconds suggests that depletion of Ca^{2+} in the local ER store underlying the puff site was minimal. Thus, it is unlikely that Ca^{2+} depletion in the ER lumen during the much briefer time course of normal puffs could be an important mechanism contributing to their termination.

3.4. Independent or coupled closings of IP_3R channels

Our objective through the remainder of this paper was to examine whether IP_3R channels close independently of one another during the falling phase of puffs, or whether their closings are correlated. For this purpose, we restricted analysis to those events that showed no apparent re-openings, and where we could resolve abrupt, stepwise decrements on the falling phase (i.e. types ii and iii puffs as classified in Fig. 2B).

For comparison with experimental data, we considered two model situations for channel closings. Firstly, an independent closing (IC) model, wherein channels close stochastically and independently following a mean open time that is identical for all channels. In this case, the falling phase of puffs is expected to display a progressive downward staircase progressing in unitary (single-channel) steps. Moreover, the average time course is expected to be exponential, with a time constant given by the mean channel open duration [28]. Secondly, we considered a more complex situation by simulating the behavior of several clustered IP_3R channels modeled using the classical De Young–Keizer scheme (see Section 2 for details). All channels were placed at the same point in space, so that each would experience the same local $[Ca^{2+}]$ and would thus exhibit maximal Ca^{2+}-mediated interaction.

3.5. Channel kinetics during the falling phase of puffs

Puffs recorded by TIRF microscopy often exhibited abrupt decrements jumping across several unitary step levels (e.g. Figs. 1C and 2B), suggesting the near-synchronous closing of several IP_3R channels. To establish whether such behavior may point to interdependence between IP_3R channel closings, or whether it may simply arise from random coincidence of independent channels that happened to close together within the time resolution of our recordings, we compared experimental data with model simulations based on independent channel kinetics.

The left column in Fig. 4A shows examples from a dataset of 30 experimental puffs in which stepwise decrements could be resolved during their falling phases. These were chosen from recordings at 17 puff sites on the basis of having monotonically decreasing falling phases (i.e. without channel re-openings), and having good signal to noise ratio, but were otherwise randomly selected. An average trace formed after aligning the 30 experimental puffs to their peak time showed a good fit to a single exponential decay, with a time constant of 49 ms (Fig. 4B, upper left panel). For comparison, we generated 30 model puffs using the IC scheme (Fig. 4A, right column), simulating idealized records considering clusters of 10 channels (approximating the amplitude distribution of the experimental puffs) which opened simultaneously and then closed stochastically and independently after a mean time of 49 ms ($k_{off} = 20.4\,s^{-1}$), and then added Gaussian noise with a standard deviation matching that of the experimental records. As expected, an average of these simulated puffs closely followed a single exponential decay, with a time constant close to 49 ms (Fig. 4B, upper right panel).

The observation of an exponential time course for the population-averaged experimental puff does not necessarily imply independent channel closings. As an extreme example, the same result would be obtained if all channels closed in synchrony to give 'square' puffs, whose durations were exponentially distributed. We thus examined deviations of individual experimental puffs from exponentially decaying time courses (Fig. 4B, lower left panel) with time constants fixed at 49 ms (red trace) or allowed to vary to produce a best fit (blue trace); and similarly determined the deviations of individual simulated puffs from an exponential time course (Fig. 4B, lower right panel). Superimposed traces plotting residual deviations from all 30 experimental and 30 simulated puffs are shown, respectively, in the left and right columns in Fig. 4C after subtracting exponentials with a fixed time constant of 49 ms (red traces) and when the time constant was allowed to vary to provide the best fit to each individual event (blue traces). In all cases the residuals were filtered by 5 point adjacent averaging to reduce background noise. By either method, the experimental puffs displayed greater deviations from exponential decay than did the simulated data. This is further demonstrated in Fig. 4D, plotting the mean variance of the respective residuals during the decay of experimental (black lines) and simulated puffs (gray lines) for variable (left) and fixed time constants (right).

As an alternative approach to examine whether the experimental data demonstrated independent or coupled closing behavior we measured the durations of the step dwell times (as illustrated in Fig. 5A) during the falling phase of the 30 experimental puffs. A plot of the mean step dwell time versus the number of channels estimated to be open during each step showed that step durations shortened only slightly with number of open channels (Fig. 5B, solid squares). This behavior is markedly different from the exponentially declining relationship expected if channel closings were independent, given that the probability that one of n open channels will close, and hence terminate a step, increases in direct proportion to n (Fig. 5B, solid circles). This is further illustrated in Fig. 5C, where the slope of a line fitted to the experimental data plotted on log–log coordinates differs appreciably from the slope of unity expected for an independent closing model. Moreover, the observed behavior also differs markedly from that predicted by a DYK simulation of channel behavior, even when all channels at the puff site were considered as a point source to maximize Ca^{2+}-mediated interactions. The open circles in Fig. 5B plot the mean dwell times at different step levels derived from simulated data, which differ from the observations even more than do the data predicted by an independent closing model. The simulated DYK model results indicate that the rate of channel closings is faster than expected from independent behavior when several channels are open, likely because high local Ca^{2+} concentrations lead to increased Ca^{2+}-inhibition.

3.6. Changes in temperature produce qualitative changes in puff time course

Increasing temperature speeds the decay of puffs (Fig. 6A), likely as a result of a shortening in mean channel open time [32]. However, we now report that temperature changes additionally cause a consistent change in the shape, not merely the rate of the puff decay. This is illustrated in Fig. 6B, showing overlaid traces of representative puffs recorded at 12 and 36 °C, after expanding the timescale of

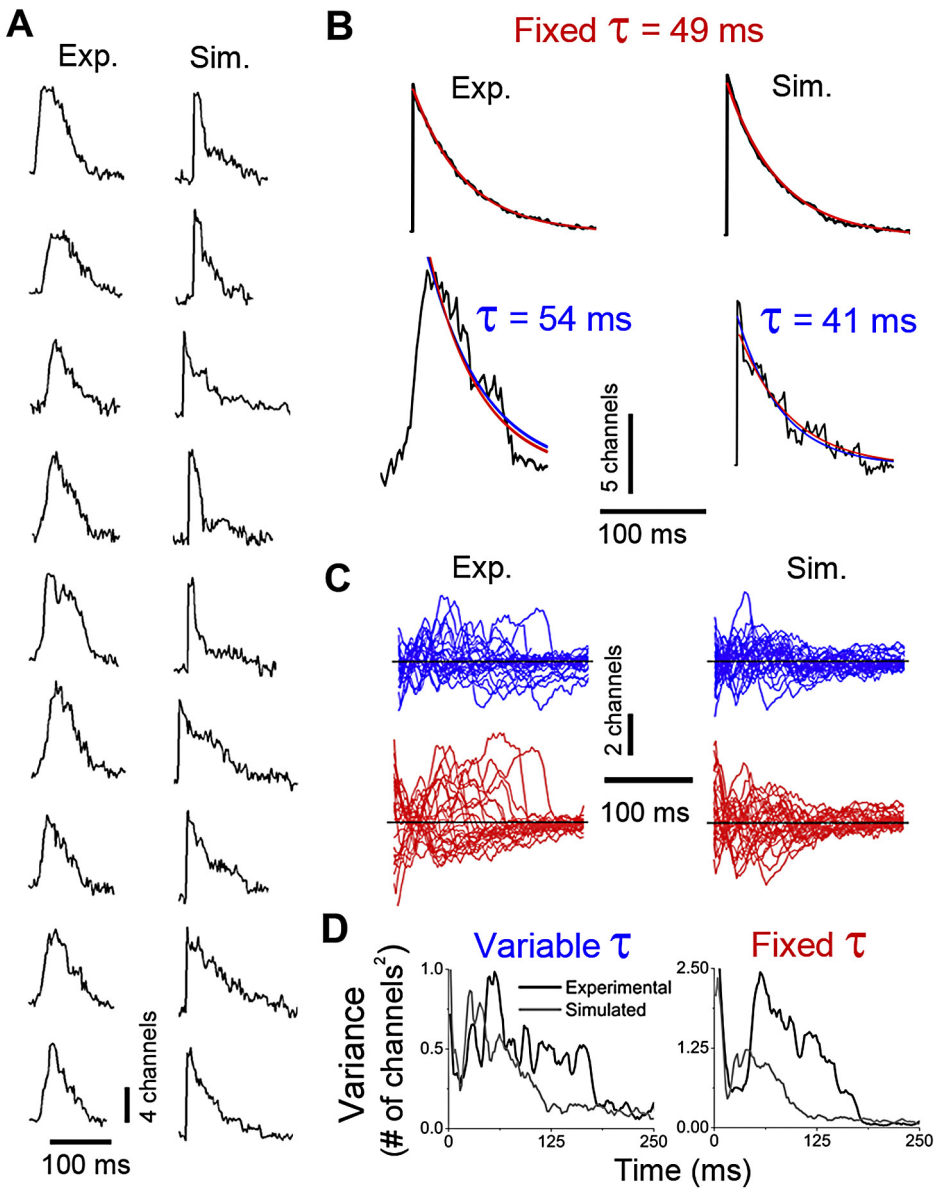

Fig. 4. Channel closings during puffs do not follow the exponential distribution predicted by an independent, stochastic gating mechanism. (A) The left panels show representative experimental records of calcium puffs, selected as showing rapid rising phases, and falling phases without obvious re-openings. The right panel shows, for comparison, simulated puffs generated by a cluster of channels that opened simultaneously and closed stochastically and independently with a mean open duration of 49 ms. Gaussian noise with a standard deviation equal to the baseline experimental noise was added to the idealized channel records. (B) Exponential fitting of puff decays. Traces on the left are experimental records, right hand traces are simulated data. Upper panels show population means (black traces) of 30 experimental and 30 simulated records like those in *A*, together with single-exponential curves (red), both with a time constant of 49 ms, which provided a good fit to the data. Black traces in the lower panels show examples of individual experimental (left) and simulated (right) puffs. Red curves are exponentials with a time constant of 49 ms; blue curves are exponentials, with time constants as indicated, providing a best fit to the records. (C) Upper panels (blue) show superimposed traces of residual differences between individual puffs (experimental, left; simulated, right) and exponential decays with time constants fitted individually to each puff. Lower panels (red) show corresponding residual differences from an exponential with fixed time constant of 49 ms. (D) Corresponding variances of the residual deviations from exponentials with varying time constants (left panel) and a fixed time constant of 49 ms (right panel). Each graph plots variances for both experimental (black lines) and simulated (gray lines) data. (For interpretation of the references to color in this figure legend, the reader is referred to the web version of the article.)

the 36 °C record and normalizing the puff amplitudes to facilitate visual comparison of their kinetics. It is apparent that the puff at 36 °C dwells for a longer fraction of its duration near its peak and then falls more abruptly as compared to the 12 °C puff. To quantify this change in shape ('squareness'), regardless of absolute kinetics, we calculated the ratio of the times for which a given puff exceeded 20% and 80% of its peak amplitude. Mean values of 80/20% ratio are plotted in Fig. 6C, showing a consistent and statistically significant increase in ratio (i.e. increasing squareness of the puff) with increasing temperature. Thus, higher temperature appears to promote increased coupling between IP_3R channels, such that multiple channels tend to stay open together and then close in more rapid succession.

3.7. *'Square' puffs do not arise from coincidental closings of independent channels*

Observations of 'square' puffs (Fig. 2B,iii) provide a dramatic example of instances where puff termination appears to involve the near-simultaneous closing of most or all IP_3R channels following an extended period while all remained open. However, given the relatively low proportion of such events (~6%; Fig. 2C) we were

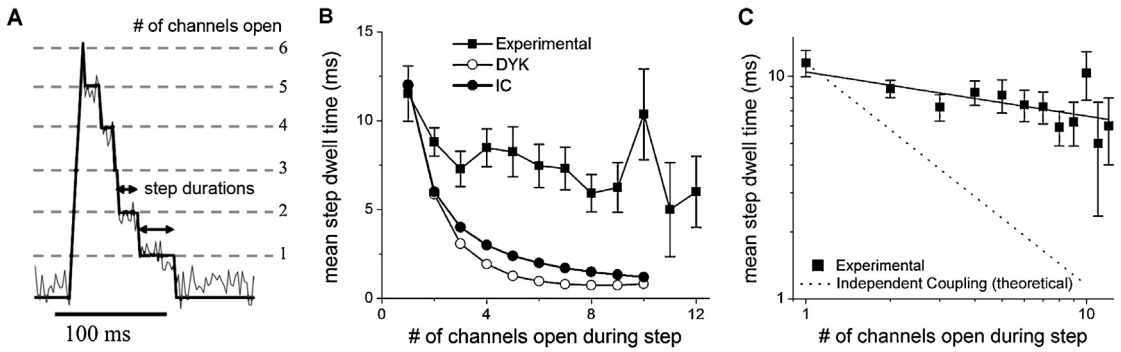

Fig. 5. Dwell-state durations during the falling phase of puffs are inconsistent with independent channel closings. (A) A representative experimental puff shown on an expanded timescale to illustrate measurements of dwell-state durations from visually identified step-levels. The number of channels open at each step was estimated by dividing the mean amplitude of the step by that of a single-channel blip (0.11 $\Delta F/F_0$). (B) Filled squares plot the mean step dwell times for 30 experimental puffs versus the estimated number of channels open during each step. Filled circles indicate the step dwell times predicted by an independent closing (IC) model, with a mean single channel dwell time of 12 ms chosen to match the observed single-channel dwell time. Open circles plot the mean dwell times predicted by a stochastic DYK simulation in which all channels in a cluster are considered as a point source. Again, the mean single channel dwell time was scaled to 12 ms. (C) The experimental data from B, re-plotted on log–log coordinates. The slope of a line fitted on these coordinates differs appreciably from the slope of unity expected if channels closed independently.

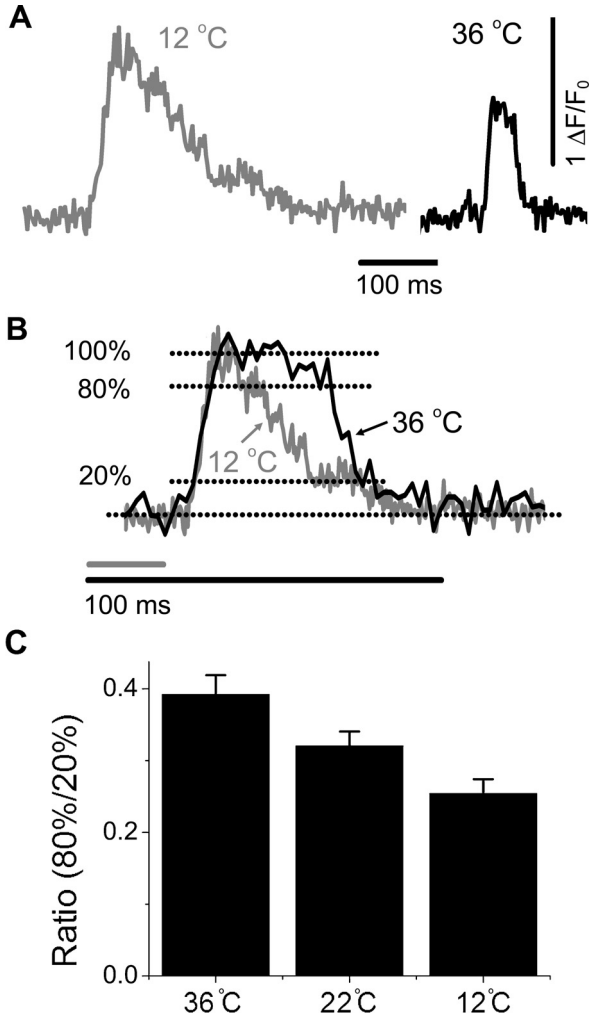

Fig. 6. Temperature-dependent changes in puff temporal morphology. (A) Representative traces showing single puffs recorded at temperatures of 12 °C (gray) and 36 °C (black), both shown at the same timescale. (B) The same records as in A, overlaid after normalizing to the same peak amplitude and with the puff at 36 °C shown on an expanded timescale (black calibration bar) to facilitate comparison of their time courses. Dashed lines illustrate measurements of puff durations at 80% and 20% of peak amplitude. (C) Ratios of puff durations at 80% and 20% amplitudes at temperatures of 36, 22 and 12 °C. Data are mean paired ratios from 50 events at each temperature. The difference between 36 and 12 °C measurements is significant at $p < 0.0001$; $p < 0.05$ comparing 22 °C measurements with other temperatures.

concerned whether they might simply arise from the coincidental, independent closing of channels within a short time of one another.

To exclude this possibility, we simulated the behavior of a point-source cluster of 5 DYK channels (chosen to match the mean number of channels estimated to open in a comparison set of experimental square puffs with mean $\Delta F/F_0 = 0.58$). We measured the interval before the first channel closes, τ_f (corresponding to duration of the plateau at the peak of the puff) and the subsequent interval between closing of the first and last channels, τ_l (corresponding to puff termination time from plateau to baseline). The ratio, τ_f/τ_l was defined as the squareness coefficient of a puff, and we defined a 'square' puff as one showing a coefficient greater than 1.0. In the experimental dataset ~8% of puffs were square, (42 out of 466 puffs with a coefficient >1.0). By comparison, simulations of the DYK model yielded <0.1% of square puffs (3 out of 3752 with a coefficient >1.0).

3.8. Coupled closings between adjacent pairs of IP_3R

To more rigorously examine the correlation between channel closings, we focused on a simplified situation, selecting sites where only two, closely adjacent IP_3R appeared to be active. We had previously shown that the number of active IP_3R at a site (estimated from the amplitude of the largest puff in relation to the unitary blip amplitude) varies considerably from site to site, with an appreciable proportion (10–15%) of sites involving just two IP_3Rs [9,30]. Representative examples from such a site are shown in Fig. 7A and B. Events occurred at two amplitude levels; $\Delta F/F_0 \sim 0.11$, corresponding to the blip amplitude [9], and $\Delta F/F_0 \sim 0.22$, which we interpret to reflect the coincident opening of two IP_3Rs. 'Double' events typically displayed an abrupt rising phase, without obvious evidence of an inflexion marking a transition from one to two open channels. Their falling phases often displayed a similarly abrupt transition back to baseline (e.g., middle trace in Fig. 7B), but in other instances a brief dwell time at the unitary amplitude level could be discerned (e.g. right-hand trace, Fig. 7B). To establish that the two channels were immediately adjacent to one another, we applied super-resolution localization by fitting two-dimensional Gaussian distributions to determine the centroid positions of the fluorescence signals during unitary and double events [31]. During the examples shown in Fig. 7B the blip (single) and double events localized to within <100 nm of one another, and although the brief duration of the unitary level step on the falling phase of the rightmost event precluded accurate localization, this nevertheless lay within ~150 nm (inset box, Fig. 7B).

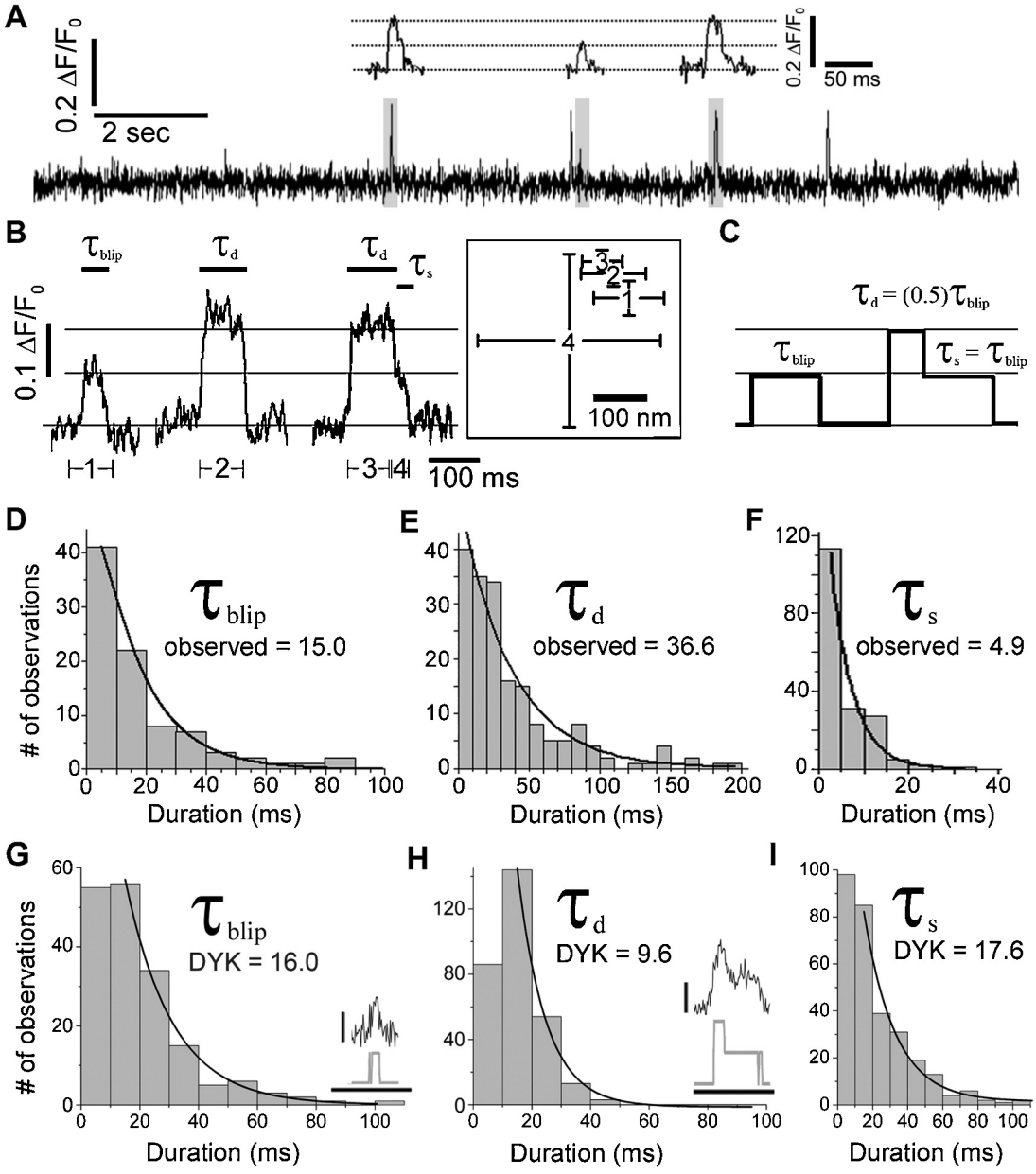

Fig. 7. Coupled closings of closely adjacent pairs of IP_3R channels. (A) The continuous trace shows a representative record from a site that displayed only single- and double-channel events. Three events marked by gray boxes are shown above on an expanded timescale, with dotted lines indicating estimated single- and double-channel fluorescence levels. (B), traces illustrating, from left to right, a single-channel opening (blip); an event that appeared to involve almost synchronous openings and closings of two channels; and an event where closing of the second channel was slightly delayed after closing of the first. As indicated, we define τ_{blip} as the single-channel open time, τ_d as the time for which two channels are simultaneously open, and τ_s as the time for which the remaining channel stays open after closure of the first. The inset shows super-resolution localization of the fluorescence centroids of these events during the time periods (1–4) indicated. Bars indicate the standard error of the localization precision. (C) Sketch illustrating the expected mean durations of τ_{blip}, τ_d and τ_s if two adjacent channels exhibited identical stochastic kinetics and closed independently. (D–F) Histograms show, respectively, the observed distributions of τ_{blip} ($N = 94$ events), τ_d ($N = 179$) and τ_s ($N = 179$), derived from experimental measurements at 13 sites. Curves are single exponential fits to the data. Mean event durations (in ms) are given based on the time constant of single-exponential fits to the observed data. (G–I) Histograms showing the respective duration distributions of τ_{blip}, τ_d and τ_s measured from fluorescence traces simulated by a stochastic model containing two DYK IP_3R channels at a point source. Curves are fitted exponentials with time constants as indicated (τ DYK). Note that X-axis scales differ from the corresponding plots in D–F. The inserts depict example traces of computer-generated single- (G) and two-channel (I) events. The lower gray traces show unprocessed channel opening data; the upper black traces show the same data after smoothing and addition of Gaussian noise to simulate fluorescence recordings and are representative of events used to obtain the distribution histograms. Scale bars are $0.1\,\Delta F/F_0$ (vertical) and 100 ms (horizontal).

We then sought to test whether the termination kinetics of double opening events were consistent with independent gating of each channel in the pair. Fig. 7C illustrates the mean dwell time durations predicted if the two channels in a pair were to close stochastically and independently (IC model), following a mean lifetime equal to that (τ_{blip}) observed during single-channel opening events. The expected dwell time of double openings (τ_d) is then given as one-half of τ_{blip} because, by definition, the double opening ends when either one of the channels close, and the rate-constant for this to occur is twice that ($1/\tau_{blip}$) for closing of a single channel. The expected mean time (τ_s) for which a remaining channel then stays open following closure of the other channel is given simply as τ_{blip} (because channel gating exhibits no 'memory', so the duration for which a channel has been open has no influence on its closing from that time onward). For simplicity, we assume that both channels opened simultaneously (e.g., opening of the second

channel is rapidly initiated by CICR following stochastic opening of the first channel), but the argument remains unchanged if we take the duration of double openings as beginning when the second channel opens, even if delayed after the first.

We obtained estimates of mean τ_{blip}, τ_d, and τ_s from measurements at 13 sites in 9 cells. Fig. 7D–F shows respective distributions of these parameters, which were all fit by single exponential decays with respective time constants of τ_{blip} 15 ms, τ_d 36.6 ms, and τ_s 4.9 ms. These observations differ markedly from those expected if closing of the channels were independent (respectively, 15, 7.5 and 15 ms). The mean duration of double openings τ_d was more than twice the mean single channel open duration τ_{blip}, whereas it would be predicted to be one-half of τ_{blip}. Moreover, the mean dwell time for which the second channel remained open following closure of the first was only about one quarter of that expected.

We also compared experimental data to results from simulations of a 2 channel, point-source cluster modeled following the DYK scheme. For a given simulation run at time $t = 0$, both channels were set to the open state, and the system evolved stochastically for 1 s. Mean values of τ_{blip}, τ_d, and τ_s derived from idealized channel records after correcting for brief flickers were, respectively, 15.0, 7.2 and 16.2 ms; in good accord with predictions of the independent closing model, but differing considerably from the experimental observations. To then further check whether limitations of the fluorescence recordings may have biased the results, we used the records of channel openings generated by the DYK scheme to simulate corresponding fluorescence traces by smoothing and addition of Gaussian noise. Dwell times (τ_{blip}, τ_d, and τ_s) were then manually measured in the same way as for the experimental records (Fig. 7G–I). Single-exponential time constants fitted to these data gave values closely similar (τ_{blip} = 16.0 ms; τ_d = 9.6 ms; τ_s = 17.6 ms) to those obtained from the idealized channel records.

We thus conclude that the gating of paired adjacent IP_3R channels is not independent, but that closing of one channel promotes the closing of the second.

4. Discussion

Calcium puffs serve autonomous localized cellular signaling functions, and act as building blocks to both trigger propagating Ca^{2+} waves and sustain the propagation of waves from one puff site to another [33–36]. Proper cellular function requires that Ca^{2+} liberation during puffs is transient, because a sustained source of cytosolic Ca^{2+}, even if spatially localized, would tend to initiate uncontrolled, repetitive waves. Thus, some mechanism is required to close IP_3R channels and terminate puffs in the face of positive feedback by CICR that would otherwise maintain Ca^{2+} release indefinitely.

We consider possible mechanisms in two categories, depending upon whether IP_3R channels close independently of one another, or whether their closings are in some way coordinated. Examples of an independent closing mechanism include binding of Ca^{2+} ions to inhibitory sites on each receptor, or dissociation of Ca^{2+} or IP_3 from activating sites. Possible examples of coupled closing mechanisms include allosteric interactions between adjacent IP_3R, and regulation of IP_3R gating via the local luminal Ca^{2+} concentration in the ER.

By utilizing TIRF microscopy of local Ca^{2+} fluorescence transients in EGTA-loaded cells we resolved the gating of individual IP_3R channels during puffs. Our observations provide several indications that channel closings during puffs are not entirely independent. Most directly, observations of 'square' puffs involving near-simultaneous closings of multiple channels from a sustained plateau level at a frequency much higher than could be accounted for by statistical chance provide a strong indication that the closing of closely adjacent IP_3R channels are not independent. A related line of evidence derives from sites containing two channels in close proximity, whose openings were coupled to one another as demonstrated by the immediate rise from baseline to a two-channel level. The synchronized openings likely arise through CICR, but involvement of other mechanisms would not invalidate our argument, which concerns only whether channel *closings* are independent or coupled. If the two channels were to close independently, the first closing is predicted to occur, on average, within a time equal to half the mean open lifetime of a single channel. The remaining time before the second channel closes should then, on average, be the same as the single channel mean lifetime. Different from this, the mean lifetime of the double-open state was more than double the single channel mean lifetime, and the mean time for closing of the remaining channel was much shorter than predicted.

We also observed a similar discrepancy for termination of puffs involving openings of several channels, by comparing experimental puff decay kinetics to simulated events generated by a model involving the independent, stochastic closings of channels. The population average of experimental puffs followed an exponential decay, but that of itself does not necessarily argue for independent channel closings. For example, the same average behavior would be observed if channels closed synchronously to give 'square' puffs whose durations were exponentially distributed. However, the decay phases of individual puffs showed greater deviations from exponential kinetics than expected from the stochastic model simulations, suggesting that channel closings were not completely independent.

What potential mechanisms might then underlie such coupling? In essence, this must involve some signal sensed in common by multiple IP_3Rs within the cluster. It is generally assumed that inhibitory feedback by the high cytosolic free $[Ca^{2+}]$ while channels are open is the major mechanism that causes IP_3R channels to close and terminate release [3]. If the spacing between IP_3R channels is appreciable as compared to the distance scale for Ca^{2+} diffusion this process may be restricted to self-inhibition. That is to say, a channel can inhibit itself, but decay of cytosolic $[Ca^{2+}]$ around an open channel is too steep for it to inhibit neighboring channels [7]. Such a mechanism is inherently independent to each channel. Conversely, if Ca^{2+} from one channel is able to inhibit neighboring channels their closing will still be stochastic, but at a rate proportional to the number of open channels: that is to say, closings will occur with higher probability at the peak of a puff when more channels are open resulting in a high local $[Ca^{2+}]$, and the rate of closings will decline as the number of open channels declines. This behavior differs from our observations of 'square' puffs when several channels remain open together and then close in near synchrony, and that the channel closing rate (step-level dwell time) shows only a slight dependence on the number of open channels (Fig. 5C). Moreover, our model simulations treating IP_3R clusters as a point source wherein each channel experiences the same local $[Ca^{2+}]$ as the others (i.e. perfect Ca^{2+} interaction between channels) gave results that differed from our observations even more than those predicted by an independent closing model (Fig. 5B). Thus, we do not believe that interactions among clustered IP_3Rs mediated by cytosolic Ca^{2+} are sufficient to explain our observations of synchronized channel closings during puffs.

Local depletion of Ca^{2+} within the ER/SR has further been proposed to play a role in the termination of puffs and sparks, either because Ca^{2+} efflux into the cytoplasm declines below the level required to sustain CICR, or through modulation of channel gating via Ca^{2+} binding to a putative receptor site on the luminal face of the channel [3,8,37]. Indeed, the first of these processes is now favored as the mechanism for spark termination [15]. However, several observations argue strongly against a local depletion as a predominant mechanism for puff termination. (i) Step-wise

decrements of fluorescence signals corresponding to closings of individual channels during the decay of puffs exhibit roughly equal magnitudes (Fig. 1B), rather than diminishing as would be expected if the driving force for single-channel Ca^{2+} efflux progressively ran-down during the course of a puff [30]. (ii) We observed instances of sustained Ca^{2+} liberation from puff sites lasting several seconds (Fig. 3), suggesting that any depletion would be minimal during typical puffs lasting only a hundred ms or less. (iii) By utilizing paired flash photorelease of IP_3, we had shown that a second puff can be evoked at a site within a few hundred ms after termination of an initial puff and that, on average, the second puff is no smaller than the first [38]. (iv) Larger puffs, involving peak openings of greater numbers of IP_3R channels on average have longer durations than smaller puffs [39], whereas the opposite result would be expected – and is indeed observed for sparks [40] – if store depletion were involved in puff termination. (v) A recent report [41] studying IP_3R channels in excised patches of nuclear membrane found no evidence for a luminal Ca^{2+} regulatory site on the IP_3R. The contrasting importance of luminal Ca^{2+} depletion during puffs vs. sparks may be accounted for because the smaller magnitude and more prolonged duration of Ca^{2+} flux during puffs would enable more efficient diffusional refilling of the local ER store underlying a puff site.

We therefore conclude that the coupled closings of IP_3Rs we observe point to some Ca^{2+}-independent process, possibly resulting from allosteric molecular interactions between channels, either direct or mediated by intermediary protein(s). This is among the first reports of such a phenomenon for IP_3R (although see Dargan et al. [42]), but analogous coupled channel gating has been reported between RyRs [16] and between clustered $Ca_v1.2$ channels [41]. Synchronized gating between RyRs incorporated into lipid bilayers was inferred based on current traces predominantly consisting of amplitudes twice the size of single channel currents, whereas little to no single channel amplitudes were observed. This coupled gating was observed only in the presence of FKBP, a protein that is tightly associated with RyR [16].

Dargan et al. [42] reported that FKBP12 coordinates the coupled gating of IP_3Rs reconstituted into lipid bilayers. Addition of rapamycin, an inhibitor of FKBP, switched the channel activity back to an independent gating scheme [42]. However, in our hands, rapamycin appeared not to disrupt the coupled closings of IP_3Rs in SH-SY5Y cells (data not shown). This difference may be methodological, given that we observed IP_3Rs in their native environment, whereas Dargan et al. [42] examined purified IP_3Rs in a lipid bilayer where modulatory proteins may have been lost. In addition, they reported that although channel openings were coupled, IP_3Rs often appeared to close independently [42]. Taylor and colleagues [43] have also reported functional coupling of gating kinetics among clustered IP_3Rs, based on patch clamp studies of IP_3Rs in the nuclear membrane showing that channels within close proximity have mean channel lifetimes that differ from 'lone' channels. They concluded that molecular interactions between IP_3Rs must account for this finding because $[Ca^{2+}]$ was clamped. However, a difference in mean channel lifetimes does not necessarily imply coupled gating; for example, it may simply reflect similar membrane environments.

Previously we reported that a typical Ca^{2+} puff likely involves synchronous openings of several IP_3R channels distributed within a cluster ~400 nm in diameter [31]. If the channels were evenly distributed this would imply an average spacing of ~100 nm, appreciably greater than the ~25 nm size of the IP_3R protein, and apparently inconsistent with our hypothesis that coupled closing of IP_3Rs involve direct protein–protein interactions. Thus, we suggest that IP_3Rs may be arranged as 'sub-groups' containing perhaps two or three intimately associated functional channels, and that these sub-groups are scattered throughout a larger region to form a puff site. Local molecular interactions at a scale of a few tens of nm may thus play important roles in terminating IP_3-mediated Ca^{2+} liberation, in addition to the longer-range (hundreds of nm to μm) actions mediated by Ca^{2+} diffusion within and between clusters to act on cytosolic regulatory sites on the IP_3R.

Conflict of interest

The authors declare that they have no conflict of interest.

Acknowledgements

This work was supported by National Institutes of Health grants GM048071 and GM 06583 to I.P., and by a University of California Systemwide Biotechnology Research and Education GREAT Training Grant (2008-14) to S.M.W.

References

[1] I. Parker, Y. Yao, Regenerative release of calcium from functionally discrete subcellular stores by inositol trisphosphate, Proc. Biol. Sci. 246 (1991) 269–274.
[2] H. Cheng, W.J. Lederer, M.B. Cannell, Calcium sparks: elementary events underlying excitation-contraction coupling in heart muscle, Science 262 (1993) 740–744.
[3] J.K. Foskett, C. White, K.H. Cheung, D.O. Mak, Inositol trisphosphate receptor Ca^{2+} release channels, Physiol. Rev. 87 (2007) 593–658.
[4] M. Iino, Biphasic Ca^{2+} dependence of inositol 1,4,5-trisphosphate-induced Ca release in smooth muscle cells of the guinea pig taenia caeci, J. Gen. Physiol. 95 (1990) 1103–1122.
[5] I. Bezprozvanny, J. Watras, B.E. Ehrlich, Bell-shaped calcium-response curves of Ins(1,4,5)P_3- and calcium-gated channels from endoplasmic reticulum of cerebellum, Nature 351 (1991) 751–754.
[6] M. Endo, Calcium-induced calcium release in skeletal muscle, Physiol. Rev. 89 (2009) 1153–1176.
[7] G. Ullah, I. Parker, D.O. Mak, J.E. Pearson, Multi-scale data-driven modeling and observation of calcium puffs, Cell Calcium 52 (2012) 152–160.
[8] M.D. Stern, H. Cheng, Putting out the fire: what terminates calcium-induced calcium release in cardiac muscle? Cell Calcium 35 (2004) 591–601.
[9] I.F. Smith, S.M. Wiltgen, I. Parker, Localization of puff sites adjacent to the plasma membrane: functional and spatial characterization of Ca^{2+} signaling in SH-SY5Y cells utilizing membrane-permeant caged IP_3, Cell Calcium 45 (2009) 65–76.
[10] A. Chu, M. Fill, E. Stefani, M.L. Entman, Cytoplasmic Ca^{2+} does not inhibit the cardiac muscle sarcoplasmic reticulum ryanodine receptor Ca^{2+} channel, although Ca^{2+}-induced Ca^{2+} inactivation of Ca^{2+} release is observed in native vesicles, J. Membr. Biol. 135 (1993) 49–59.
[11] S. Gyorke, P. Velez, B. Suarez-Isla, M. Fill, Activation of single cardiac and skeletal ryanodine receptor channels by flash photolysis of caged Ca^{2+}, Biophys. J. 66 (1994) 1879–1886.
[12] R. Sitsapesan, A.J. Williams, Gating of the native and purified cardiac SR Ca^{2+}-release channel with monovalent cations as permeant species, Biophys. J. 67 (1994) 1484–1494.
[13] D.R. Laver, L.D. Roden, G.P. Ahern, K.R. Eager, P.R. Junankar, A.F. Dulhunty, Cytoplasmic Ca^{2+} inhibits the ryanodine receptor from cardiac muscle, J. Membr. Biol. 147 (1995) 7–22.
[14] A. Schiefer, G. Meissner, G. Isenberg, Ca^{2+} activation and Ca^{2+} inactivation of canine reconstituted cardiac sarcoplasmic reticulum Ca^{2+}-release channels, J. Physiol. 489 (Pt 2) (1995) 337–348.
[15] M.D. Stern, E. Rios, V.A. Maltsev, Life and death of a cardiac calcium spark, J. Gen. Physiol. 142 (2013) 257–274.
[16] S.O. Marx, K. Ondrias, A.R. Marks, Coupled gating between individual skeletal muscle Ca^{2+} release channels (ryanodine receptors), Science 281 (1998) 818–821.
[17] S.O. Marx, J. Gaburjakova, M. Gaburjakova, C. Henrikson, K. Ondrias, A.R. Marks, Coupled gating between cardiac calcium release channels (ryanodine receptors), Circ. Res. 88 (2001) 1151–1158.
[18] D.O. Mak, J.E. Pearson, K.P. Loong, S. Datta, M. Fernandez-Mongil, J.K. Foskett, Rapid ligand-regulated gating kinetics of single inositol 1,4,5-trisphosphate receptor Ca^{2+} release channels, EMBO Rep. 8 (2007) 1044–1051.
[19] J. Shuai, I. Parker, Optical single-channel recording by imaging Ca^{2+} flux through individual ion channels: theoretical considerations and limits to resolution, Cell Calcium 37 (2005) 283–299.
[20] S. Swillens, G. Dupont, L. Combettes, P. Champeil, From calcium blips to calcium puffs: theoretical analysis of the requirements for interchannel communication, Proc. Natl. Acad. Sci. U.S.A. 96 (1999) 13750–13755.
[21] J.W. Shuai, P. Jung, Optimal intracellular calcium signaling, Phys. Rev. Lett. 88 (2002) 068102.
[22] R. Hinch, A mathematical analysis of the generation and termination of calcium sparks, Biophys. J. 86 (2004) 1293–1307.
[23] J.R. Groff, G.D. Smith, Calcium-dependent inactivation and the dynamics of calcium puffs and sparks, J. Theor. Biol. 253 (2008) 483–499.

[24] I. Bezprozvanny, B.E. Ehrlich, Inositol (1,4,5)-trisphosphate ($InsP_3$)-gated Ca channels from cerebellum: conduction properties for divalent cations and regulation by intraluminal calcium, J. Gen. Physiol. 104 (1994) 821–856.
[25] P.J. Perez, J. Ramos-Franco, M. Fill, G.A. Mignery, Identification and functional reconstitution of the type 2 inositol 1,4,5-trisphosphate receptor from ventricular cardiac myocytes, J. Biol. Chem. 272 (1997) 23961–23969.
[26] R.E. Hagar, A.D. Burgstahler, M.H. Nathanson, B.E. Ehrlich, Type III $InsP_3$ receptor channel stays open in the presence of increased calcium, Nature 396 (1998) 81–84.
[27] A. Demuro, I. Parker, Optical patch-clamping: single-channel recording by imaging Ca^{2+} flux through individual muscle acetylcholine receptor channels, J. Gen. Physiol. 126 (2005) 179–192.
[28] G. Solovey, D. Fraiman, S.P. Dawson, Mean field strategies induce unrealistic non-linearities in calcium puffs, Front. Physiol. 2 (2011) 46.
[29] D. Swaminathan, G. Ullah, P. Jung, A simple sequential-binding model for calcium puffs, Chaos. 19 (2009) 037109.
[30] G.D. Dickinson, D. Swaminathan, I. Parker, The probability of triggering calcium puffs is linearly related to the number of inositol trisphosphate receptors in a cluster, Biophys. J. 102 (2012) 1826–1836.
[31] S.M. Wiltgen, I.F. Smith, I. Parker, Superresolution localization of single functional IP_3R channels utilizing Ca^{2+} flux as a readout, Biophys. J. 99 (2010) 437–446.
[32] G.D. Dickinson, I. Parker, Temperature dependence of IP_3-mediated local and global Ca^{2+} signals, Biophys. J. 104 (2013) 386–395.
[33] M.J. Berridge, Elementary and global aspects of calcium signalling, J. Exp. Biol. 200 (1997) 315–319.
[34] N. Callamaras, J.S. Marchant, X.P. Sun, I. Parker, Activation and co-ordination of $InsP_3$-mediated elementary Ca^{2+} events during global Ca^{2+} signals in *Xenopus* oocytes, J. Physiol. 509 (Pt. 1) (1998) 81–91.
[35] S.P. Dawson, J. Keizer, J.E. Pearson, Fire-diffuse-fire model of dynamics of intracellular calcium waves, Proc. Natl. Acad. Sci. U.S.A. 96 (1999) 6060–6063.
[36] J. Marchant, N. Callamaras, I. Parker, Initiation of IP_3-mediated Ca^{2+} waves in *Xenopus* oocytes, EMBO J. 18 (1999) 5285–5299.
[37] D. Fraiman, S.P. Dawson, A model of IP_3 receptor with a luminal calcium binding site: stochastic simulations and analysis, Cell Calcium 35 (2004) 403–413.
[38] N. Callamaras, I. Parker, Phasic characteristic of elementary Ca^{2+} release sites underlies quantal responses to IP_3, EMBO J. 19 (2000) 3608–3617.
[39] I.F. Smith, I. Parker, Imaging the quantal substructure of single IP_3R channel activity during Ca^{2+} puffs in intact mammalian cells, Proc. Natl. Acad. Sci. U.S.A. 106 (2009) 6404–6409.
[40] S.Q. Wang, M.D. Stern, E. Rios, H. Cheng, The quantal nature of Ca^{2+} sparks and in situ operation of the ryanodine receptor array in cardiac cells, Proc. Natl. Acad. Sci. U.S.A. 101 (2004) 3979–3984.
[41] H. Vais, J.K. Foskett, G. Ullah, J.E. Pearson, D.O. Daniel Mak, Permeant calcium ion feed-through regulation of single inositol 1,4,5-trisphosphate receptor channel gating, J. Gen. Physiol. 140 (2012) 697–716.
[42] S.L. Dargan, E.J. Lea, A.P. Dawson, Modulation of type-1 $Ins(1,4,5)P_3$ receptor channels by the FK506-binding protein, FKBP12, Biochem. J. 361 (2002) 401–407.
[43] R. Taufiq Ur, A. Skupin, M. Falcke, C.W. Taylor, Clustering of $InsP_3$ receptors by $InsP_3$ retunes their regulation by $InsP_3$ and Ca^{2+}, Nature 458 (2009) 655–659.